Available online at www.sciencedirect.com
SCIENCE DIRECT®
International Journal of Heat and Mass Transfer 48 (2005) 2697–2707
International Journal of HEAT and MASS TRANSFER
www.elsevier.com/locate/ijhmt

Prediction of heat transfer coefficient on the fin inside one-tube plate finned-tube heat exchangers

Han-Taw Chen *, Jen-Pin Song, Yi-Tong Wang

Department of Mechanical Engineering, National Cheng Kung University, Tainan 701, Taiwan

Received 12 July 2004; received in revised form 31 January 2005
Available online 28 March 2005

Abstract

The finite difference method in conjunction with the least-squares scheme and the experimental temperature data is proposed to predict the average heat transfer coefficient and the fin efficiency on the fin inside one-tube plate finned-tube heat exchangers for various air speeds and the temperature difference between the ambient temperature and the tube temperature. Previous works showed that the heat transfer coefficient on this rectangular fin is very non-uniform. Thus the whole plate fin is divided into several sub-fin regions in order to predict the average heat transfer coefficient and the fin efficiency on the fin from the knowledge of the fin temperature recordings at several selected measurement locations. The results show that the surface heat flux and the heat transfer coefficient on the upstream region of the fin can be markedly higher than those on the downstream region. The fin temperature distributions depart from the ideal isothermal situation and the fin temperature decreases more rapidly away from the circular center, when the frontal air speed increases. The average heat transfer coefficient on the fin increases with the air speed and the temperature difference between the ambient temperature and the tube temperature. This implies that the effect of the temperature difference between the tube temperature and the ambient temperature is not negligent.

1. Introduction

The fins in heat exchangers are always applied to increase the heat flow per unit of basic surface. The analysis of a continuous plate fin pierced by a regularly spaced array of circular tubes in staggered and in-line arrays has many engineering applications. In order to simplify the problem considered, the calculation of the standard fin efficiency usually assumes that the heat transfer coefficient is constant over the plate fin. Many investigators [1–3] also applied various analytical and numerical methods to obtain the fin efficiency under the assumption of the uniform heat transfer coefficient. However, it is well known that there exists a very complex flow pattern within a plate finned-tube heat exchanger due to its three-dimensional nature and flow separations. The flow accelerates around the tube and forms a low-velocity wake region behind the tube. This causes local variations of the heat transfer coefficient, as shown in Refs. [4–7]. Jones and Russell [4], Saboya and Sparrow [5], Rosman et al. [6] and Ay et al. [7] demonstrated that there exists the great variation of the heat transfer rate on the fin inside a plate finned-tube heat exchanger. On the other hand, the heat transfer coefficient on the fin is very non-uniform. This also implies that the actual steady-state heat transfer coefficient on the fin

* Corresponding author. Fax: +886 6 235 2973.
E-mail address: htchen@mail.ncku.edu.tw (H.-T. Chen).

0017-9310/$ - see front matter © 2005 Elsevier Ltd. All rights reserved.
doi:10.1016/j.ijheatmasstransfer.2005.01.035

Nomenclature

A_f	area of the whole plate fin, m^2
A_j	area of the jth sub-fin region, m^2
$[A]$	global conduction matrix
d_o	outer diameter of a tube, m
$[F]$	force matrix
h	local heat transfer coefficient, W/m^2 K
$\bar{h}$	unknown average heat transfer coefficient on the whole plate fin, W/m^2 K
$\bar{h}_j$	unknown average heat transfer coefficient on the jth sub-fin region, W/m^2 K
k	thermal conductivity of the fin, W/m K
L	side length of a square plate fin, m
ℓ	distance between two neighboring nodes in the x- and y-directions
m	dimensionless parameter defined in Eq. (5)
$\bar{m}_j$	unknown dimensionless parameter on the jth sub-fin region defined in Eq. (10)
N	number of temperature measurements on the fin
N_x	number of nodes in the x-direction
N_y	number of nodes in the y-direction
Q	total heat flux dissipated from the whole plate fin, W
q_j	heat flux dissipated from the jth sub-fin region, W
Re_d	Reynolds number
r_o	outer radius of the circular tube, m
S_1	outer boundary surface of the circular tube
T	temperature
T_j	temperature measurement on the jth sub-fin region
T_o	outer surface temperature of the circular tube
T_∞	ambient temperature
ΔT	temperature difference, $T_o - T_\infty$
V_{air}	frontal air speed, m/s
X, Y	spatial coordinates, m
x, y	dimensionless spatial coordinates

Greek symbols

δ	fin thickness
η_f	fin efficiency
v	kinematic viscosity of the air, m^2/s
θ	temperature difference, $T - T_\infty$
$[\theta]$	global temperature matrix

Superscripts

cal	calculated value
mea	measured data

inside a plate finned-tube heat exchanger should be the function of position. As shown in Ref. [8], the measurements of the local heat transfer coefficient on plain fins under steady-state heat transfer conditions are very difficult to perform, since the local fin temperature and local heat flux are required. Thus the estimation of a more accurate heat transfer coefficient on the fin is an important task for the device of the high-performance heat exchangers.

Quantitative studies of the heat transfer processes occurring in the industrial applications require accurate knowledge of the surface conditions and the thermal physical quantities of the material. It is well known that these physical quantities and the surface conditions can be predicted using the temperature measurements inside the material. Such problems are called the inverse heat conduction problems and have become an interesting subject recently. To date, various inverse methods in conjunction with the measured temperatures inside the material have been developed for the analysis of the inverse heat conduction problems [9,10]. However, to the authors' knowledge, a few investigators performed the prediction of the local heat transfer coefficients on the fin inside the plate finned-tube heat exchangers.

Maillet et al. [11] applied the analytical and boundary element methods to predict the heat transfer coefficient on a cylinder. Lin et al. [12,13] used the finite-difference method in conjunction with the linear least-squares scheme to estimate the space-variable heat transfer coefficient on a heated cylinder normal to the laminar and turbulent air streams. Owing to the requirement of the local fin temperature measurements, the estimations of the local heat transfer coefficients on the plate fin under steady-state heat transfer conditions are generally more difficult than that on the boundary surface of a physical geometry, as shown in Refs. [11–13]. Thus a few researchers predicted the distribution of the local heat transfer coefficients on a plate fin [4–7,14]. Jones and Russell [4] applied the transient technique to determine the local heat transfer coefficient on the rectangular fin pierced by an elliptical steel tube and then the finite element method was used to calculate its fin efficiency. Saboya and Sparrow [5] and Rosman et al. [6] cast solid naphthalene plates in the form of a plate-fin-and-tube flow passage and used mass transfer techniques to infer the local heat transfer coefficients from the heat-mass transfer analogy. The local mass transfer coefficients were defined by measuring the thickness of naphthalene lost by sublimation during a timed test run. Recently,

Ay et al. [7] performed an experimental study with the infrared thermovision to monitor the temperature distribution on a plate-fin surface inside the plate finned-tube heat exchangers, and then the local heat transfer coefficients on the tested fin can be determined using the obtained experimental temperature measurements. Huang et al. [14] applied the steepest descent method and a general purpose commercial code CFX4.4 to estimate the local heat transfer coefficients for the plate finned-tube heat exchangers based on the simulated measured temperature distributions on the fin surface by infrared thermography. However, the difference of the local heat transfer coefficients in the wake and frontal regions of the tube and the fin efficiency on the fin inside the plate finned-tube heat exchangers were not shown in the works of Ay et al. [7] and Huang et al. [14]. Sometimes, it is maybe difficult to measure the temperature distributions on the fin of plate finned-tube heat exchangers using the infrared thermography and the thermocouples for some practical heat transfer problems. Under the circumstance, the present scheme can be introduced for such problems.

The inverse analysis of the present study is that the whole fin area is divided into several analysis sub-fin regions and then the fin temperatures at these selected measurement locations are measured using K-type thermocouples. Afterwards, the finite difference method in conjunction with these temperature measurements and the least-squares method is applied to predict the average heat transfer coefficients on these sub-fin regions. Furthermore, the average heat transfer coefficient on the whole plate fin $\bar{h}$ and the fin efficiency can be obtained for various frontal air speeds under the given conditions of the ambient temperature and the tube temperature.

The advantage of the present study is that the governing differential equations for the airflow do not need to be solved. In this study, the effect of the temperature difference between the ambient temperature and the tube temperature on the estimation of the $\bar{h}$ value will be investigated. The computational procedure for the estimates of the heat transfer coefficients on each sub-fin region is performed repeatedly until the sum of the squares of the deviations between the calculated and measured temperatures becomes minimum.

2. Mathematical formulation

The schematic diagram of the one-tube plate fin heat exchanger is shown in Fig. 1. Fig. 2 shows the physical model of the two-dimensional thin plate fin inside a one-tube plate fin heat exchanger, where r_o, L and δ denote the outer radius of the circular tube, the side length of the square plane fin and the fin thickness, respectively. The circular tube is located at $(L/2, L/2)$. T_o and T_∞ respectively denote the surface temperature of the circular tube and the ambient temperature. Owing to the thin fin behavior, the temperature gradient in the z-direction (the fin thickness) is small and the fin temperature varies only in the X- and Y-directions. The "insulated tip" assumption can be an adequate approximation provided that the actual heat flux dissipated through the tip is much smaller than the total heat flux drawn from the base wall. It can be found from the works of Jones and Russell [4], Saboya and Sparrow [5], Rosman et al. [6] and Ay et al. [7] that the heat transfer coefficient on the fin inside the plate fin heat exchangers is very non-uniform. Thus the heat transfer coefficient $h(X, Y)$ in the present study is also assumed to be non-uniform. The heat transfer coefficient on the fin inside a plate finned-tube heat exchanger can be estimated provided that the fin temperatures at various measurement

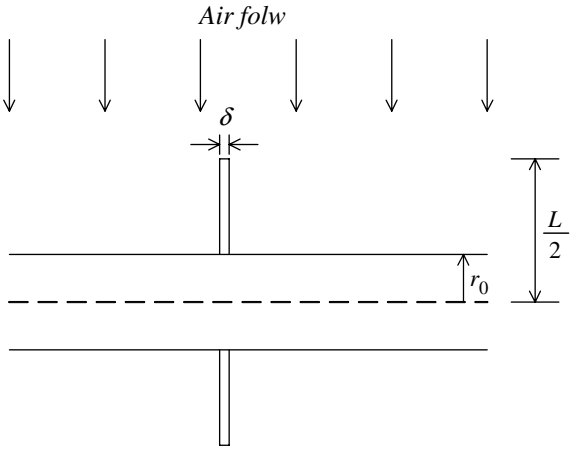

Fig. 1. Schematic diagram of one-tube plate fin heat exchanger.

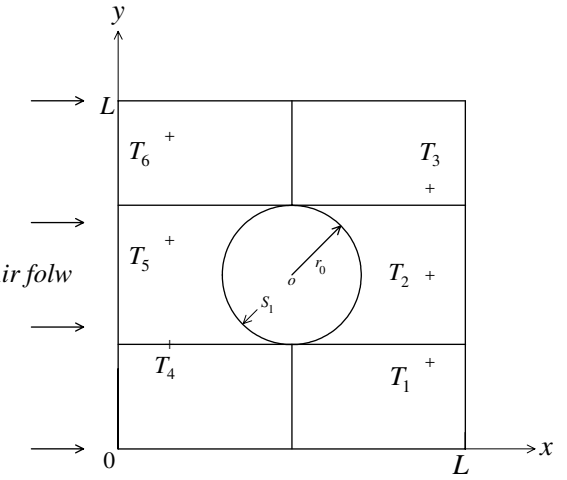

Fig. 2. Physical geometry of two-dimensional plate fin with a circular tube.

locations can be measured. Under the assumptions of the steady state and the constant thermal properties, the two-dimensional heat conduction equation for the continuous thin fin inside a plate finned-tube heat exchanger can be expressed as

$$\frac{\partial^2 T}{\partial X^2}+\frac{\partial^2 T}{\partial Y^2}=\frac{2h(X,Y)}{k\delta}(T-T_\infty) \tag{1}$$

Its corresponding boundary conditions are

$$\frac{\partial T}{\partial X}=0 \quad \text{at } X=0 \text{ and } X=L \tag{2}$$

$$\frac{\partial T}{\partial Y}=0 \quad \text{at } Y=0 \text{ and } Y=L \tag{3}$$

$$T=T_{\mathrm{o}} \quad (X,Y) \text{ on } S_1 \tag{4}$$

where T is the fin temperature. X and Y are Cartesian coordinates. S_1 denotes the boundary of the circular tube with radius r_{o}. k is the thermal conductivity of the fin.

For convenience of the inverse analysis, the following dimensionless parameters are introduced as

$$x=X/L, \quad y=Y/L \quad \text{and} \quad m(x,y)=\frac{2L^2h(x,y)}{k\delta} \tag{5}$$

Substitution of Eq. (5) into Eqs. (1)–(4) gives the following equations.

$$\frac{\partial^2\theta}{\partial x^2}+\frac{\partial^2\theta}{\partial y^2}=m(x,y)\theta \tag{6}$$

$$\frac{\partial\theta}{\partial x}=0 \quad \text{at } x=0 \text{ and } x=1 \tag{7}$$

$$\frac{\partial\theta}{\partial y}=0 \quad \text{at } y=0 \text{ and } y=1 \tag{8}$$

and

$$\theta=0 \quad (x,y) \text{ on } S_1 \tag{9}$$

where $\theta = T - T_\infty$.

3. Numerical analysis

In the present study, the whole plate fin is divided into N sub-fin regions. The heat transfer coefficient on each sub-fin region is assumed to be constant. Thus the application of the finite difference method to Eq. (6) can produce the following difference equation on the kth sub-fin region as

$$\frac{\theta_{i+1,j}-2\theta_{i,j}+\theta_{i-1,j}}{\ell^2}+\frac{\theta_{i,j+1}-2\theta_{i,j}+\theta_{i,j-1}}{\ell^2} =\bar{m}_k\theta_{i,j} \quad \text{for } k=1,2,\ldots,N \tag{10}$$

where ℓ is the distance between two neighboring nodes in the x- and y-directions and is defined as $\ell = 1/(N_x - 1) = 1/(N_y - 1)$, where N_x and N_y are the nodal numbers in x- and y-directions, respectively. $\bar{m}_k$ denotes the unknown dimensionless parameter on the kth sub-fin region and is defined as $\bar{m}_k = 2L^2\bar{h}_k/(k\delta)$, where $\bar{h}_k$ denotes the average heat transfer coefficient on the kth sub-fin region.

The application of the central difference approximation to the boundary conditions (7) and (8) can yield their approximate forms as

$$\theta_{2,j}=\theta_{0,j} \quad \text{and} \quad \theta_{N_x-1,j}=\theta_{N_x+1,j} \quad \text{for } j=1,2,\ldots,N_y \tag{11}$$

$$\theta_{i,2}=\theta_{i,0} \quad \text{and} \quad \theta_{i,N_y-1}=\theta_{i,N_y+1} \quad \text{for } i=1,2,\ldots,N_x \tag{12}$$

Substitution of Eqs. (11) and (12) into their corresponding difference equations can obtain the difference equations at the boundary surfaces as

$$\frac{2\theta_{2,j}-2\theta_{1,j}}{\ell^2}+\frac{\theta_{1,j+1}-2\theta_{1,j}+\theta_{1,j-1}}{\ell^2}=\bar{m}_k\theta_{1,j} \quad \text{for } k=4,5,6 \tag{13}$$

$$\frac{-2\theta_{N_x,j}+2\theta_{N_x-1,j}}{\ell^2}+\frac{\theta_{N_x,j+1}-2\theta_{N_x,j}+\theta_{N_x,j-1}}{\ell^2}=\bar{m}_k\theta_{N_x,j} \quad \text{for } k=1,2,3 \tag{14}$$

$$\frac{\theta_{i+1,1}-2\theta_{i,1}+\theta_{i-1,1}}{\ell^2}+\frac{2\theta_{i,2}-2\theta_{i,1}}{\ell^2}=\bar{m}_k\theta_{i,1} \quad \text{for } k=1,4 \tag{15}$$

and

$$\frac{\theta_{i+1,N_y}-2\theta_{i,N_y}+\theta_{i-1,N_y}}{\ell^2}+\frac{-2\theta_{i,N_y}+2\theta_{i,N_y-1}}{\ell^2}=\bar{m}_k\theta_{i,N_y} \quad \text{for } k=3,6 \tag{16}$$

It can be found from Refs. [3,15] that the boundary of the circular tube may be approximated in terms of a Cartesian coordinate system. Thus a more accurate modified difference equation based on this technique will be constructed in the present study.

The difference equations for the nodes at the interface of two neighboring sub-fin regions, as shown in Fig. 3, can be expressed as

$$\frac{\theta_{i+1,j}-2\theta_{i,j}+\theta_{i-1,j}}{\ell^2}+\frac{\theta_{i,j+1}-2\theta_{i,j}+\theta_{i,j-1}}{\ell^2} =\frac{\bar{m}_k+\bar{m}_{k+1}}{2}\theta_{i,j} \tag{17}$$

Rearrangement of Eq. (10) and Eqs. (13)–(17) in conjunction with the difference equations in the neighboring of the circular tube can yield the following matrix equation.

$$[A][\theta]=[F] \tag{18}$$

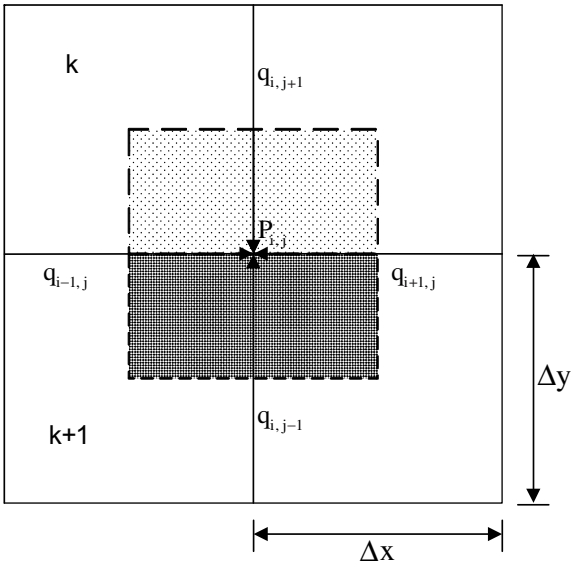

Fig. 3. Nodes for the interface of two-neighboring sub-fin areas.

where $[A]$ is a global conduction matrix. $[\theta]$ is a matrix representing the nodal temperatures. $[F]$ is a force matrix. The nodal temperatures can be obtained from Eq. (18) by using the Gauss elimination method.

However, it is maybe difficult to measure the temperature distributions on the whole plate fin using the infrared thermography and the thermocouples for some practical heat transfer problems. Relatively, the unknown local heat transfer coefficient on the fin $h(x,y)$ is not easy to be obtained. Under this circumstance, the whole plate fin considered can be divided into several sub-fin regions in the present inverse scheme and then the unknown heat transfer coefficient on each sub-fin region can be approximated by a constant value. Under this assumption, the heat flux dissipated from this sub-fin region q_j is

$$q_j = \bar{h}_j \int_{A_i} (T - T_\infty)\,\mathrm{d}A \quad \text{for } j = 1,2,\ldots,N \tag{19}$$

The average heat transfer coefficient on the whole plate fin $\bar{h}$ can be expressed as

$$\bar{h} = \sum_{j=1}^{N} \bar{h}_j A_j / A_\mathrm{f} \tag{20}$$

where N is the total number of the sub-fin regions. A_f is the area of the whole plate fin.

The efficiency of the continuous plate fin η_f is defined as the ratio of the actual heat transfer from the continuous plate fin to the dissipated heat from the fin maintained at the tube temperature T_o. Thus the fin efficiency η_f can be expressed as

$$\eta_\mathrm{f} = \frac{\sum_{j=1}^{N} q_\mathrm{j}}{A_\mathrm{f}(T_\mathrm{o} - T_\infty)\bar{h}} \tag{21}$$

The total heat flux dissipated from the whole plate fin to the ambient Q can be written as

$$Q = \sum_{j=1}^{N} q_j = \eta_\mathrm{f} A_\mathrm{f} \tag{22}$$

In order to estimate the unknown heat transfer coefficient on the jth sub-fin region $\bar{h}_j$, the additional information of the steady-state temperature measurements is required at N interior measurement locations. The more a number of the sub-fin regions are, the more accurate the estimation of the unknown average heat transfer coefficient on the whole plate fin is. Relatively, a more computational time can be required. In the present study, K-type thermocouples are used to record the temperature information at selected measurement locations. The temperature measurement taken from the jth thermocouple at the measurement location x_j is denoted by T_j^mea $(j = 1,\ldots,N)$, as shown in Tables 1 and 2.

The least-squares minimization technique is applied to minimize the sum of the squares of the deviations between the calculated temperatures and the temperature measurements at selected measurement locations. The error in the estimates $E(\bar{m}_1,\bar{m}_2,\ldots,\bar{m}_N)$ will be minimized. $E(\bar{m}_1,\bar{m}_2,\ldots,\bar{m}_N)$ is defined as

$$E(\bar{m}_1,\bar{m}_2,\ldots,\bar{m}_N) = \sum_{j=1}^{N} [\theta_j^\mathrm{cal} - \theta_j^\mathrm{mea}]^2 \tag{23}$$

where the unknown average heat transfer coefficient on each sub-fin region h_i, $i = 1,2,\ldots,N$, can be obtained from the definition of $\bar{m}_i$. The calculated temperature at $x = x_j, \theta_j^\mathrm{cal}$, is taken from Eq. (18). The temperature θ_j^mea is defined as $\theta_j^\mathrm{mea} = T_j^\mathrm{mea} - T_\infty$.

The estimated values of $\bar{m}_i$, $i = 1,2,\ldots,N$, are determined until the value of $E(\bar{m}_1,\bar{m}_2,\ldots,\bar{m}_N)$ is minimum. The computational procedures for estimating the $\bar{m}_i$ value, $i = 1,2,\ldots,N$, are described as follows.

First, the initial guesses of $\bar{m}_i$, $i = 1,2,\ldots,N$, are arbitrarily chosen. Accordingly, the calculated temperature at $x = x_j$, θ_j^cal, can be determined. Deviation of θ_j^mea and θ_j^cal, e_j, is expressed as

$$e_j = \theta_j^\mathrm{cal} - \theta_j^\mathrm{mea} \quad \text{for } j = 1,2,\ldots,N \tag{24}$$

The new calculated temperature $\theta_j^{\mathrm{cal},n}$ can be expanded in a first-order Taylor series as

$$\theta_j^{\mathrm{cal},n} = \theta_j^\mathrm{cal} + \sum_{i=1}^{N} \frac{\partial \theta_j^\mathrm{cal}}{\partial \bar{m}_i}\mathrm{d}\bar{m}_i \quad \text{for } j = 1,2,\ldots,N \tag{25}$$

In order to obtain the $\frac{\partial \theta_j^\mathrm{cal}}{\partial \bar{m}_i}$ value, the new estimated value $\bar{m}_i^*$ is introduced and is expressed as

Table 1
Temperature measurements and the present estimates for various V_{air} values, $T_o = 59.6\ ^\circ C$ and $T_\infty = 25.6\ ^\circ C$

	$V_{air} = 1$ m/s	$V_{air} = 2$ m/s	$V_{air} = 3$ m/s	$V_{air} = 4$ m/s	$V_{air} = 5$ m/s
T_j^{mea} (°C)	$T_1^{mea} = 42.3$	$T_1^{mea} = 39.8$	$T_1^{mea} = 38.0$	$T_1^{mea} = 36.8$	$T_1^{mea} = 35.8$
	$T_2^{mea} = 46.0$	$T_2^{mea} = 41.4$	$T_2^{mea} = 39.8$	$T_2^{mea} = 39.5$	$T_2^{mea} = 37.8$
	$T_3^{mea} = 41.7$	$T_3^{mea} = 38.8$	$T_3^{mea} = 36.0$	$T_3^{mea} = 35.2$	$T_3^{mea} = 34.2$
	$T_4^{mea} = 38.5$	$T_4^{mea} = 36.1$	$T_4^{mea} = 34.6$	$T_4^{mea} = 33.2$	$T_4^{mea} = 32.7$
	$T_5^{mea} = 36.1$	$T_5^{mea} = 35.4$	$T_5^{mea} = 32.3$	$T_5^{mea} = 31.3$	$T_5^{mea} = 30.8$
	$T_6^{mea} = 35.6$	$T_6^{mea} = 34.9$	$T_6^{mea} = 30.3$	$T_6^{mea} = 30.1$	$T_6^{mea} = 30.0$
$\bar{h}_j$ (W/m^2 K)	$\bar{h}_1 = 12.9$	$\bar{h}_1 = 11.72$	$\bar{h}_1 = 15.37$	$\bar{h}_1 = 19.68$	$\bar{h}_1 = 20.01$
	$\bar{h}_2 = 6.19$	$\bar{h}_2 = 18.13$	$\bar{h}_2 = 20.55$	$\bar{h}_2 = 19.63$	$\bar{h}_2 = 26.73$
	$\bar{h}_3 = 13.88$	$\bar{h}_3 = 14.67$	$\bar{h}_3 = 22.76$	$\bar{h}_3 = 27.33$	$\bar{h}_3 = 28.62$
	$\bar{h}_4 = 2.75$	$\bar{h}_4 = 10.32$	$\bar{h}_4 = 5.52$	$\bar{h}_4 = 7.00$	$\bar{h}_4 = 6.68$
	$\bar{h}_5 = 60.15$	$\bar{h}_5 = 64.71$	$\bar{h}_5 = 98.98$	$\bar{h}_5 = 120.96$	$\bar{h}_5 = 134.73$
	$\bar{h}_6 = 13.24$	$\bar{h}_6 = 14.36$	$\bar{h}_6 = 32.47$	$\bar{h}_6 = 31.27$	$\bar{h}_6 = 30.62$
$q_j \times 10^{-4}$ (W)	$q_1 = 4020$	$q_1 = 3329$	$q_1 = 4137$	$q_1 = 4982$	$q_1 = 4907$
	$q_2 = 2157$	$q_2 = 5881$	$q_2 = 6363$	$q_2 = 5972$	$q_2 = 7897$
	$q_3 = 4071$	$q_3 = 3945$	$q_3 = 5228$	$q_3 = 6046$	$q_3 = 6107$
	$q_4 = 796$	$q_4 = 2607$	$q_4 = 1375$	$q_4 = 1628$	$q_4 = 1530$
	$q_5 = 17{,}707$	$q_5 = 18{,}350$	$q_5 = 26{,}437$	$q_5 = 31{,}545$	$q_5 = 34{,}815$
	$q_6 = 3248$	$q_6 = 3399$	$q_6 = 6170$	$q_6 = 5790$	$q_6 = 5606$
$\bar{h}$ (W/m^2 K)	17.76	21.77	31.83	36.71	40.1
$Q \times 10^{-4}$ (W)	31,999	37,511	49,710	55,963	60,861
η_f	61%	58%	53%	51%	51%

Table 2
Temperature measurements and the present estimates for various V_{air} values, $T_o = 69.5\ ^\circ C$ and $T_\infty = 26.5\ ^\circ C$

	$V_{air} = 1$ m/s	$V_{air} = 2$ m/s	$V_{air} = 3$ m/s	$V_{air} = 4$ m/s	$V_{air} = 5$ m/s
T_j^{mea} (°C)	$T_1^{mea} = 45.0$	$T_1^{mea} = 42.1$	$T_1^{mea} = 39.8$	$T_1^{mea} = 38.8$	$T_1^{mea} = 37.6$
	$T_2^{mea} = 49.2$	$T_2^{mea} = 46.2$	$T_2^{mea} = 43.4$	$T_2^{mea} = 42.4$	$T_2^{mea} = 40.1$
	$T_3^{mea} = 44.5$	$T_3^{mea} = 41.8$	$T_3^{mea} = 38.8$	$T_3^{mea} = 37.3$	$T_3^{mea} = 35.4$
	$T_4^{mea} = 41.2$	$T_4^{mea} = 36.8$	$T_4^{mea} = 36.3$	$T_4^{mea} = 35.0$	$T_4^{mea} = 33.0$
	$T_5^{mea} = 38.0$	$T_5^{mea} = 33.7$	$T_5^{mea} = 33.0$	$T_5^{mea} = 31.8$	$T_5^{mea} = 31.1$
	$T_6^{mea} = 37.1$	$T_6^{mea} = 33.5$	$T_6^{mea} = 32.5$	$T_6^{mea} = 31.1$	$T_6^{mea} = 30.3$
$\bar{h}_j$ (W/m^2 K)	$\bar{h}_1 = 14.89$	$\bar{h}_1 = 18.28$	$\bar{h}_1 = 21.68$	$\bar{h}_1 = 23.87$	$\bar{h}_1 = 23.28$
	$\bar{h}_2 = 10.81$	$\bar{h}_2 = 15.69$	$\bar{h}_2 = 21.69$	$\bar{h}_2 = 23.54$	$\bar{h}_2 = 23$
	$\bar{h}_3 = 15.39$	$\bar{h}_3 = 18.53$	$\bar{h}_3 = 24.98$	$\bar{h}_3 = 30.54$	$\bar{h}_3 = 36.35$
	$\bar{h}_4 = 2.72$	$\bar{h}_4 = 3.02$	$\bar{h}_4 = 1.92$	$\bar{h}_4 = 1.87$	$\bar{h}_4 = 9.94$
	$\bar{h}_5 = 71.92$	$\bar{h}_5 = 124.81$	$\bar{h}_5 = 137.57$	$\bar{h}_5 = 166.28$	$\bar{h}_5 = 187.48$
	$\bar{h}_6 = 16.53$	$\bar{h}_6 = 24.13$	$\bar{h}_6 = 27.65$	$\bar{h}_6 = 34.91$	$\bar{h}_6 = 40.56$
$q_j \times 10^{-4}$ (W)	$q_1 = 5505$	$q_1 = 6169$	$q_1 = 6897$	$q_1 = 7331$	$q_1 = 6734$
	$q_2 = 4565$	$q_2 = 6299$	$q_2 = 8291$	$q_2 = 8802$	$q_2 = 11568$
	$q_3 = 5343$	$q_3 = 5843$	$q_3 = 7119$	$q_3 = 8140$	$q_3 = 9009$
	$q_4 = 957$	$q_4 = 946$	$q_4 = 594$	$q_4 = 556$	$q_4 = 2625$
	$q_5 = 25{,}978$	$q_5 = 41{,}736$	$q_5 = 45{,}507$	$q_5 = 53{,}818$	$q_5 = 59{,}182$
	$q_6 = 4788$	$q_6 = 6069$	$q_6 = 6580$	$q_6 = 7767$	$q_6 = 8627$
$\bar{h}$ (W/m^2 K)	21.49	33.04	38.1	45.46	53.37
$Q \times 10^{-4}$ (W)	47,139	67,085	74,987	86,413	97,746
η_f	58%	54%	52%	51%	49%

$$\bar{m}_i^* = \bar{m}_i + \mathrm{d}_i \delta_{ik} \quad \text{for } i,k = 1,2,\ldots,N \tag{26}$$

where $\mathrm{d}_i = \bar{m}_i^* - \bar{m}_i$ denotes the correction. The symbol δ_{jk} is Kronecker delta.

Accordingly, the new calculated temperature $\theta_j^{cal,n}$ with respect to $\bar{m}_i^*$ can be determined from Eq. (18). Deviation of $\theta_j^{cal,n}$ and θ_j^{mea}, e_j^n, can be defined as

$$e_j^n = \theta_j^{\mathrm{cal},n} - \theta_j^{\mathrm{mea}} \quad \text{for } j = 1,2,\ldots,N \tag{27}$$

The finite difference representation of the derivative $\frac{\partial \theta_j^{\mathrm{cal}}}{\partial \bar{m}_i}$ can be expressed as

$$\omega_j^i = \frac{\partial \theta_j^{\mathrm{cal}}}{\partial \bar{m}_i} = \frac{\theta_j^{\mathrm{cal},n} - \theta_j^{\mathrm{cal}}}{\bar{m}_i^* - \bar{m}_i} \quad \text{for } j = 1,2,\ldots,N \tag{28}$$

Substitution of Eqs. (24), (26) and (27) into Eq. (28) can yield

$$\omega_j^i = \frac{e_j^n - e_j}{d_i} \quad \text{for } j = 1,2,\ldots,N \tag{29}$$

Substitution of Eq. (28) into Eq. (25) can obtain the new expression of $\theta_j^{\mathrm{cal},n}$ as

$$\theta_j^{\mathrm{cal},n} = \theta_j^{\mathrm{cal}} + \sum_{i=1}^{N} \omega_j^i \mathrm{d}_i^* \quad \text{for } j = 1,2,\ldots,N \tag{30}$$

where $\mathrm{d}_i^* = \mathrm{d}\bar{m}_i$ denotes the new correction for the values of $\bar{m}_i$.

Substituting Eqs. (24) and (27) into Eq. (30) gives

$$e_j^n = e_j + \sum_{i=1}^{N} \omega_j^i \mathrm{d}_i^* \quad \text{for } j = 1,2,\ldots,N \tag{31}$$

As shown in Eq. (23), the error in the estimates $E(\bar{m}_1 + \Delta\bar{m}_1, \bar{m}_2 + \Delta\bar{m}_2, \ldots, \bar{m}_N + \Delta\bar{m}_N)$ can be expressed as

$$\mathbf{E} = \sum_{j=1}^{N} (e_j^n)^2 \tag{32}$$

In order to yield the minimum value of $\mathbf{E}$ with respect to the $\bar{m}_i$ values, differentiating $\mathbf{E}$ with respect to the new correction d_i^* will be performed. Thus the correction equations for the $\bar{m}_i$ values can be expressed as

$$\sum_{j=1}^{N} \sum_{k=1}^{N} \omega_k^i \omega_k^j \mathrm{d}_j^* = -\sum_{j=1}^{N} \omega_j^i e_j \quad i = 1,2,\ldots,N \tag{33}$$

Eq. (33) is a set of N algebraic equations for the new corrections. The new correction d_i^* can be obtained by solving Eq. (33). Furthermore, the new estimated heat transfer coefficients can also be determined. The above procedures are repeated until the values of $\left|\frac{\theta_j^{\mathrm{mea}} - \theta_j^{\mathrm{cal}}}{\theta_j^{\mathrm{mea}}}\right|$, $j = 1,2,\ldots,N$, are all less than 10^{-4}.

4. Experimental problem

The present experiments were conducted in an induced open wind tunnel as shown in Fig. 2 of Ref. [16]. This setup is based on ASHRAE 41.2 standard [17]. The ambient temperature was controlled by an air-ventilator that can provide a cooling capacity up to 21.2 kW. The ambient airflow was driven by a 3.73 kW centrifugal fan with an inverter to provide various inlet velocities. The airflow measuring station is an outlet chamber setup with multiple nozzle based on ASHRAE 41.1 standard [18]. The frontal air speeds ranged from 0.3 to 6.5 m/s. The air temperatures at the inlet and the exit zones across the test section were measured by two psychometric boxes, which are constructed based on ASHRAE 41.1 standard [18]. The working medium in the tube was the hot or chilled water. The water temperature was controlled by a thermostat reservoir. The inlet temperatures of the hot and chilled waters were controlled at 75 °C for the dry condition and at 7.0 °C for the wet condition, respectively. Both the inlet and outlet temperatures of the water were measured by two precalibrated RTDs. Their accuracy was to within 0.05 °C. The tube temperature T_o in the present study is assumed to be the average of the inlet and outlet water temperatures. The water volumetric flow rate was measured by a magnetic volume flow meter with 0.002 l/s resolution. For the present problem, the flow and thermal fields in the previous works were often assumed to be symmetric. In order to investigate the reliability of the above assumption and the effect of the thermocouple locations on the average heat transfer coefficient and the fin efficiency, the irregular arrangement of the thermocouples welded on the fin is chosen. Thus the fin heat transfer area is divided into six regions due to the consideration of the flow pattern. Regions 2 and 5 respectively are the wake fin area and upstream fin area. Regions 4–6 are the leading edge area of the fin. In order to estimate the average heat transfer coefficient on each sub-fin region, six K-type thermocouples are welded at the suitable positions of the sub-fin region. These six K-type thermocouples for the measurements of the fin temperature are respectively welded at (0.9, 0.25), (0.9, 0.5), (0.9, 0.75), (0.15, 0.3), (0.15, 0.6) and (0.15, 0.9). It can be observed that the first and third thermocouples are symmetric with respect to $y = L/2$. The diameter of the spot sizes of these six thermocouples is about 1.2 mm. The readings of the thermocouples used to measure the fin temperatures are recorded when the steady-state condition has reached. All the data signals were collected and converted by a data acquisition system (a Yokogawa Hybrid Recorder DR 240). The data acquisition system then transmitted the converted signals through a GPIB interface to the host computer for further operation. During the experiments, the inlet water temperature was held constant. In general, the energy balance between the air side and the tube side was ±3% for dry coils and ±7% for wet coils.

The circular tube with an outer diameter of 40 mm and 2 mm in thickness and the tested plate fin with 100 mm in length, 100 mm in width and 2 mm in thickness are made of AISI 304 stainless material. It can be found from Ref. [16] that the thermal conductivity of AISI 304 stainless material is 14.9 W/m K. As shown in Ref. [19], the "insulated tip" assumption is a good approximation when the actual heat flux passed through

the tip is negligible relative to the total heat flux drawn from the base wall. For simplicity, the average heat transfer coefficient on the tip surface can be assumed to be the same as that on the lateral surfaces of the fin. On the other hand, the "insulated tip" assumption will be reasonable provided that the surface area of the fin tip is very smaller than the total fin surface area. Their ratio for the present study can be written as $\frac{2\delta L}{(L^2-\pi r_0^2)+2\delta L}$. Based on the experiment data given in the present study, the surface area of the fin tip is only 4.37% of the total fin surface area. This implies that the heat flux passed through the fin tip can be neglected in the present study. Thus Eqs. (2) and (3) in the present study should be the reasonable assumptions. In this study, the Reynolds number Re_d is defined as $Re_d = V_{air} d_o/v$, where V_{air}, d_o and v denote the frontal air speed, the outer diameter of the circular tube and the kinematic viscosity of the air. This implies that the Re_d value ranges about from 2500 to 13,000. It can be seen from Ref. [8] that the airflow in the present problem can become turbulent for $V_{air} \geqq 4$ m/s. The values of $T_1^{mea}(0.9, 0.25)$, $T_2^{mea}(0.9, 0.5)$, $T_3^{mea}(0.9, 0.75)$, $T_4^{mea}(0.15, 0.3)$, $T_5^{mea}(0.15, 0.6)$ and $T_6^{mea}(0.15, 0.9)$ respectively denote T_1^{mea}, T_2^{mea}, T_3^{mea}, T_4^{mea}, T_5^{mea} and T_6^{mea}. These temperature measurements for various frontal air speeds under the given conditions of the tube temperature T_o and the ambient temperature T_∞ are shown in Tables 1 and 2. Tables 1 and 2 also show the effect of the frontal air speed V_{air} on the average heat transfer coefficient on the jth sub-fin region $\bar{h}_j$, heat flux on the jth sub-fin region q_j, total heat flux on the whole plate fin Q, the average heat transfer coefficient on the whole plate fin $\bar{h}$ and the fin efficiency η_f. An interesting finding from Tables 1 and 2 is that the T_1^{mea} value does not equal the T_3^{mea} value. This phenomenon can result from that the wavy flow behind the tube has become turbulent and random in motion. Thus the symmetric assumptions of the flow and thermal fields are not always very reasonable for the present problem. In addition, it can be found from Tables 1 and 2 that the fin temperatures on the downstream fin region are markedly higher than those on the upstream region for various air speeds under the given conditions of T_o and T_∞. Due to the blockade of the tube, the maximum heat transfer coefficient and heat flux occur on the upstream fin region. This implies that Region 2 makes a big contribution to the whole heat transfer coefficient. This higher heat transfer coefficient also becomes large as the value of "$T_o - T_\infty$" is increased. It is expected because the higher value of "$T_o - T_\infty$" will induce the higher heat removal rate. In general, the average heat transfer coefficient is very low on the back surface of the tube or on the downstream fin region, as shown in Tables 1 and 2. On the other hand, there exists a low-performance wake region behind the tube. Evidently, Region 2 contributes a little to the heat transfer performance of the heat exchanger. Therefore, in order to enhance the overall heat transfer, it is worth to find a way to increase heat transfer in the region 2. This may lead to design a heat exchanger with a high heat transfer performance. The ratio of the average heat transfer coefficient in the front region $\bar{h}_5$ to that in the wake region $\bar{h}_2$ at $V_{air} = 1$ m/s is up to 10 times for $\Delta T = 34$ °C ($T_o = 59.6$ °C and $T_\infty = 25.6$ °C) and is 7 times for $\Delta T = 43$ °C ($T_o = 69.5$ °C and $T_\infty = 26.5$ °C), where $\Delta T = T_o - T_\infty$ is defined as the temperature difference between the tube temperature T_o and the ambient temperature T_∞. As stated by Rosman et al. [6], the heat transfer coefficient is very low on the back surface of the tube and is much higher in the entrance than in the wake region. The ratio of the heat flux in the front region q_5 to that in the wake region q_2 at $V_{air} = 1$ m/s is about 8.2 times for $\Delta T = 34$ °C and is about 5.7 times for $\Delta T = 43$ °C. It can be observed from Tables 1 and 2 that the average heat transfer coefficient on the forth sub-fin area $\bar{h}_4$ is smaller than that on other sub-fin areas. The occurrence of this phenomenon may result from the error of the temperature measurements, its corresponding thermocouple position located at the interface between the forth sub-fin region and the fifth sub-fin region and other uncertain experimental factors. The $\bar{h}$ value for $\Delta T = 43$ °C is approximately 33% greater than that for $\Delta T = 34$ °C at $V_{air} = 5$ m/s. However, the Q value for $\Delta T = 43$ °C is up to 61% greater than that for $\Delta T = 34$ °C at $V_{air} = 5$ m/s. Thus the effect of ΔT on $\bar{h}$ and Q is not negligent. The results in Tables 1 and 2 show that the wake downstream region of a one-tube finned-tube heat exchanger in the range of $V_{air} = 1$–5 m/s is responsible for 6–16% of the total heat flux on the whole plate fin when $\Delta T = 34$ °C and for 9–12% when $\Delta T = 43$ °C. It can be found from the work of Rosman et al. [6] that the wake downstream region of the tube row is responsible for 13–14% of the total heat transferred by the fin. Obviously, the present estimates agree with those of Rosman et al. [6]. Figs. 4 and 5 respectively show the effect of the frontal air speed V_{air} or the Reynolds number Re_d on the average heat transfer coefficient on the whole plate fin $\bar{h}$ and the fin efficiency η_f. The smoothing straight lines are applied to match the data points of $\bar{h} - V_{air}$ and $\eta_f - V_{air}$. The functional forms of these straight lines can be obtained by using the least-square fitting method of experimental data and are expressed as

$$\bar{h} = \begin{cases} 5.962V_{air} + 11.748 & \text{for } \Delta T = 34\,^\circ\text{C} \\ 7.618V_{air} + 15.438 & \text{for } \Delta T = 43\,^\circ\text{C} \end{cases} \tag{34}$$

and

$$\eta_f = \begin{cases} -0.0265V_{air} + 0.6283 & \text{for } \Delta T = 34\,^\circ\text{C} \\ -0.0227V_{air} + 0.5956 & \text{for } \Delta T = 43\,^\circ\text{C} \end{cases} \tag{35}$$

It can be observed from Figs. 4 and 5 that, at the same air speed, the average heat transfer coefficient $\bar{h}$ increases

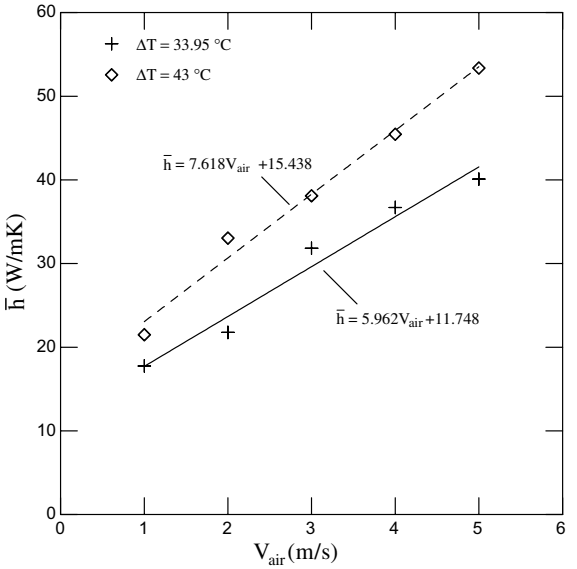

Fig. 4. Variation of $\bar{h}$ with V_{air} under various ΔT conditions.

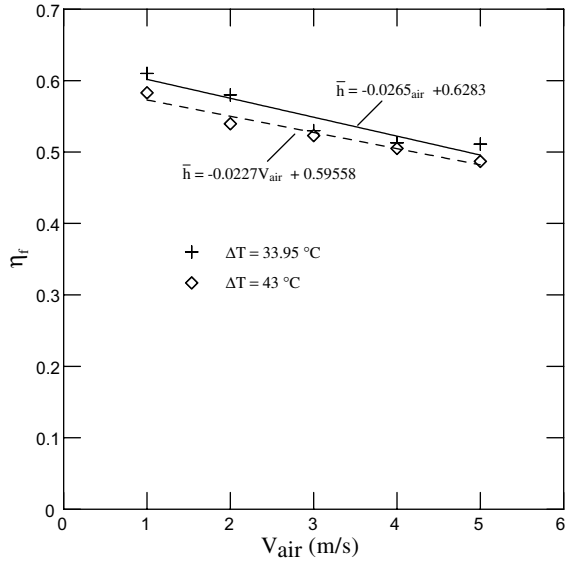

Fig. 5. Variation of η_f with V_{air} under various ΔT conditions.

with the ΔT value and the fin efficiency decreases with increasing the ΔT value. However, the effect of ΔT on $\bar{h}$ and η_f did not obviously be shown in the works of Rosman et al. [6] and Ay et al. [7]. In addition, the average heat transfer coefficient $\bar{h}$ also increases with the V_{air} value or Re_d. The $\bar{h}$ value in the range of V_{air} = 1–5 m/s increases from 17.76 W/m^2 K to 41 W/m^2 K for ΔT = 34 °C and increases from 21.5 W/m^2 K to 53.4 W/m^2 K for ΔT = 43 °C. It can be found from the work of Ay et al. [7] that the $\bar{h}$ value increases from 17.8 W/m^2 K to 20 W/m^2 K at V_{air} = 1 m/s for the plate finned-tube heat exchangers with the in-line tube arrangements. It is obvious that the present estimates of $\bar{h}$ agree with those of Ay et al. [7]. The fin efficiency η_f in the range of V_{air} = 1–5 m/s decreases with increasing the V_{air} value or Re_d. The η_f value decreases from 60% to 50% for ΔT = 34 °C and k = 14.9 W/m K and decreases from 58% to 48% for ΔT = 43 °C and k = 14.9 W/m K. It can be found from the work of Rosman et al. [6] that the η_f value for the one-tube row configuration decreases with increasing the Reynolds number and decreases from 81% to 61% for k = 62 W/m K and from 92.4% to 82.7% for k = 202 W/m K. These results show that the η_f value also decreases with the thermal conductivity of the tested material. Thus, it is reasonable that the present estimates of η_f are smaller than those given by Rosman et al. [6].

Once the average heat transfer coefficient on each sub-fin region can be obtained, the temperature distribution on the whole plate fin can also be determined from Eq. (18). Figs. 6 and 7 show the calculated temperature distributions on the whole plate fin for ΔT = 34 °C (T_o = 59.6 °C and T_∞ = 25.6 °C) and various air speeds. The calculated temperature distributions on the fin for ΔT = 43 °C (T_o = 69.5 °C and T_∞ = 26.5 °C) and various air speeds are shown in Figs. 8 and 9. It can be observed from Figs. 6–9 that there is a considerable temperature drop between the tube wall and the edge of the plate fin owing to the poor thermal conductivity of the steel fin. The fin temperature distributions obviously depart from the ideal isothermal situation and the fin temperature decreases more rapidly away from the circular center when the frontal air speed increases.

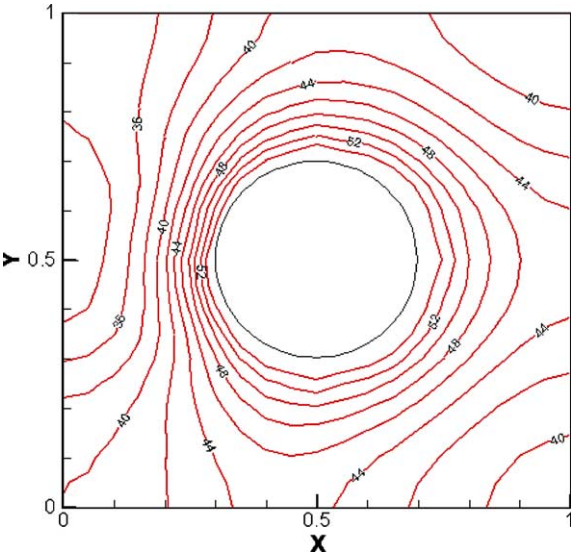

Fig. 6. Distribution of the calculated fin temperature for T_o = 59.6 °C, T_∞ = 25.6 °C and V_{air} = 1 m/s.

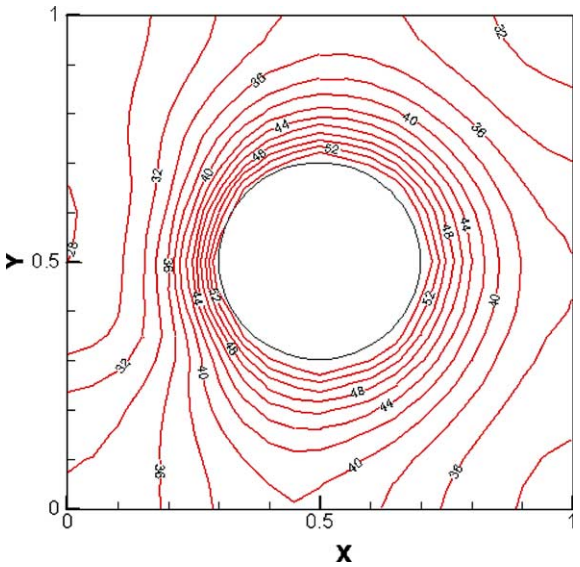

Fig. 7. Distribution of the calculated fin temperature for T_o = 59.6 °C, T_∞ = 25.6 °C and V_{air} = 5 m/s.

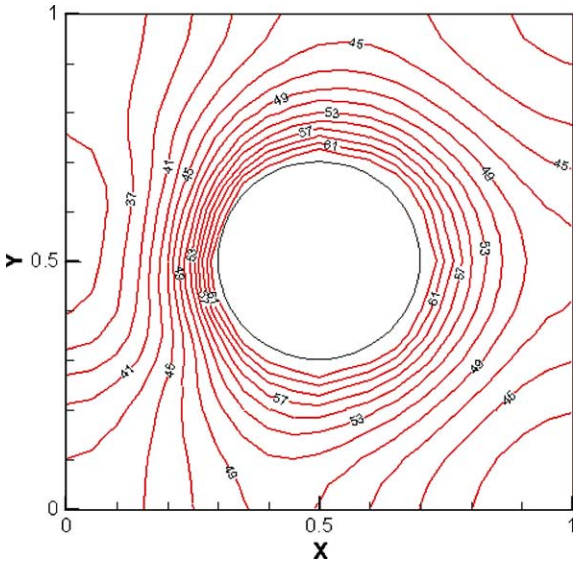

Fig. 8. Distribution of the calculated fin temperature for T_o = 69.5 °C, T_∞ = 26.5 °C and V_{air} = 1 m/s.

Owing to the above phenomenon, the fin efficiency decreases with increasing the frontal air speed or the Reynolds number.

5. Conclusions

The present study proposes a numerical inverse scheme involving the finite difference method in conjunction with the least-squares method and the experimental fin temperatures at six measurement locations to estimate the unknown heat transfer coefficients on six sub-fin regions, the average heat transfer coefficient on the whole plate fin $\bar{h}$ and the fin efficiency η_f for various air speeds under the given conditions of the tube temperatures T_o and the ambient temperature T_∞. The estimated results show that the fin temperature distributions depart from the ideal isothermal situation and the fin temperature decreases more rapidly away from the circular center, when the frontal air speed increases. The average heat transfer coefficients are very low on the back surface of the tube. The ratio of the average heat transfer coefficient in the front region to that in the wake region can be up to 10 times under the given conditions of V_{air}, T_o and T_∞. The $\bar{h}$ value increases with the frontal air speed V_{air}. However, the η_f value decreases with increasing the V_{air} value. The greater the ΔT value is, the greater the $\bar{h}$ value is and the smaller the η_f value is. It is worth mentioning that the effect of the temperature difference between the tube temperature and the ambient temperature on the $\bar{h}$ value and the total heat flux on the whole plate fin is not negligent.

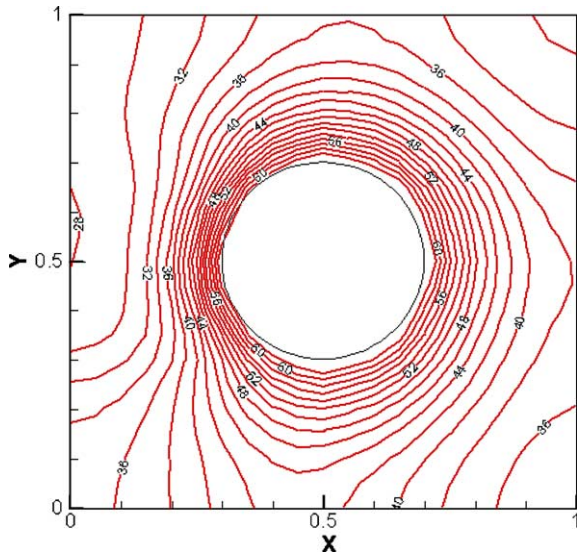

Fig. 9. Distribution of the calculated fin temperature for T_o = 69.5 °C, T_∞ = 26.5 °C and V_{air} = 5 m/s.

Acknowledgements

The authors gratefully acknowledge the financial support provided by the National Science Council of the Republic of China under Grant no. NSC 84-2212-E006-045. The authors also wish to thank Professor J.Y. Jang for giving us the support of his experimental equipments.

References

[1] H. Zabronsky, Temperature distribution and efficiency of a heat exchanger using square fins on round tubes, ASME J. Appl. Mech. 22 (1955) 119–122.

[2] D.Y. Kuan, R. Aris, H.T. Davis, Estimation of fin efficiencies of regular tubes arrayed in circumferential fins, Int. J. Heat Mass Transfer 27 (1984) 148–151.

[3] H.T. Chen, J.T. Liou, Optimum dimensions of the continuous plate fin for various tube arrays, Numer. Heat Transfer A 34 (1998) 151–167.

[4] T.V. Jones, C.M.B. Russell, Efficiency of rectangular fins, ASME/AIChE National Heat Transfer Conference, Orlando, Florida, 1980, pp. 27–30.

[5] F.E.M. Saboya, E.M. Sparrow, Local and average heat transfer coefficients for one-row plate fin and tube heat exchanger configurations, ASME J. Heat Transfer 96 (1974) 265–272.

[6] E.C. Rosman, P. Carajilescov, F.E.M. Saboya, Performance of one- and two-row tube and plate fin heat exchangers, ASME J. Heat Transfer 106 (1984) 627–632.

[7] H. Ay, J.Y. Jang, J.N. Yeh, Local heat transfer measurements of plate finned-tube heat exchangers by infrared thermography, Int. J. Heat Mass Transfer 45 (2002) 4069–4078.

[8] R.L. Webb, Principles of Enhanced Heat Transfer, Wiley, New York, 1994, pp. 125–153.

[9] M.N. Özisik, Heat Conduction, second ed., Wiley, New York, 1993 (Chapter 14).

[10] K. Kurpisz, A.J. Nowak, Inverse Thermal Problems, Computational Mechanics Publications, Southampton, UK, 1995.

[11] D. Maillet, A. Degiovanni, R. Pasquetti, Inverse heat conduction applied to the measurement of heat transfer coefficient on a cylinder: Comparison between an analytical and a boundary element technique, ASME J. Heat Transfer 113 (1991) 549–557.

[12] J.H. Lin, C.K. Chen, Y.T. Yang, An inverse estimation of the thermal boundary behavior of a heated cylinder normal to a laminar air stream, Int. J. Heat Mass Transfer 43 (2000) 3991–4001.

[13] J.H. Lin, C.K. Chen, Y.T. Yang, An inverse method for simultaneous estimation of the center and surface thermal behavior of a heated cylinder normal to a turbulent air stream, ASME J. Heat Transfer 124 (2000) 601–608.

[14] C.H. Huang, I.C. Yuan, H. Ay, A three-dimensional inverse problem in imaging the local heat transfer coefficients for plate finned-tube heat exchangers, Int. J. Heat Mass Transfer 46 (2003) 3629–3638.

[15] V.S. Arpaci, S.H. Kao, A. Selamet, Introduction to Heat Transfer, Prentice-Hall, NJ, 1999, pp. 202–205.

[16] J.Y. Jang, J.Y. Yang, Experimental and 3-D numerical analysis of the thermal–hydraulic characteristics of elliptic finned-tube heat exchangers, Heat Transfer Eng. 19 (1998) 55–67.

[17] ASHRAE Standard 41.2-1986, Standard Method for Temperature Measurement, American Society of Heating, Refrigerating and Air-Conditioning Engineers, Atlanta, GA, 1986.

[18] ASHRAE Standard 41.1-1986, Standard Method for Temperature Measurement, American Society of Heating, Refrigerating and Air-Conditioning Engineers, Atlanta, GA, 1986.

[19] A. Bejan, Heat Transfer, John Wiley & Sons Inc., New York, 1993, pp. 53–62.